FireAntV3: A Modular Self-Reconfigurable Robot Toward Free-Form Self-Assembly Using Attach-Anywhere Continuous Docks

Petras Swissler , Member, IEEE, and Michael Rubenstein

Abstract—FireAntV3 uses a refined version of the 3D Continuous Docks to attach to other such docks at any location at any orientation with simple control and without alignment. The robot improves upon previous FireAnt-series robots by redesigning the locomotion drive system to improve mechanical and attachment reliability while also reducing the number of motors from six to three. We also expand the sensory capabilities of FireAntV3 to enable the robot to sense forces, sense the direction to a light source, and to sense contacting neighbors using vibrations. We validate this robot through full-robot tests demonstrating phototaxis and neighbor-detecting behavior. This letter also describes the method for manufacturing the continuous docks in a variety of geometries.

Index Terms—Cellular and modular robots, mechanism design, swarm robotics.

I. INTRODUCTION

ELF-ASSEMBLY in social insects [1], [2], [3], [4] is a fascinating example of organisms adapting to their environment. This process involves the insects joining their bodies and following simple, distributed behaviors to create structures that benefit the swarm; the adaptability this enables would be highly advantageous for robotic systems. Robotic self-assembly is therefore seen as a promising avenue for robots to operate in unsafe, poorly understood, and dynamic environments such as disaster relief, exploration, and construction [5], [6].

Robotic self-assembling systems must overcome three key challenges: first, robots must strongly attach to each other; second, robots must move to positions that extend or grow the structure; finally, robots must decide at what location to actually grow the structure. Interestingly, traditional approaches towards meeting these challenges in robotic self-assembling systems diverge from the approaches observed in most biological systems. This hardware-focused paper primarily considers the first two of these challenges; robot sensing capabilities are informed by our prior work exploring the third challenge [7].

Manuscript received 23 February 2023; accepted 14 June 2023. Date of publication 29 June 2023; date of current version 6 July 2023. This letter was recommended for publication by Associate Editor S. Hauert and Editor M. Ani Hsieh upon evaluation of the reviewers' comments. This work was supported by the NSF IIS under Grant 1956019. (Corresponding author: Petras Swissler.)

Petras Swissler is with the Department of Mechanical and Industrial Engineering, New Jersey Institute of Technology, Newark, NJ 07102 USA (e-mail: petras.swissler@njit.edu).

Michael Rubenstein is with the Department of Computer Science and the Department of Mechanical Engineering, Northwestern University, Evanston, IL 60208 USA (e-mail: rubenstein@northwestern.edu).

This letter has supplementary downloadable material available at https://doi.org/10.1109/LRA.2023.3290796, provided by the authors.

Digital Object Identifier 10.1109/LRA.2023.3290796

Addressing the first challenge of self-assembly requires the development of attachment mechanisms. These attachment mechanisms not only influence robot design, but also define the overall organization of the self-assembled structures and thus suitability to self-assembly at large scales. Most work on robotic self-assembling systems (especially work preceding the original FireAnt robot [8]) focuses on self-assembly using discrete attachment locations [9], [10]. These fixed attachment points force the overall robotic structure to conform to a lattice, which is much different from the organization of biological self-assembling systems where insects grab each other at seemingly arbitrary locations [11], [12]. A drawback to a latticed approach is that misalignments between robots due to tolerance stack [13] can prevent successful attachments [14], [15], [16]. Typical approaches to circumvent this problem include passive alignment hardware [17], [18], sensors [19], [20], or having a highly deformable robot [21]. These added features increase the cost and complexity of the robot design and would not be necessary if robots were able to attach arbitrarily. Supporting arbitrary attachment locations also enables greater agent heterogeneity, adaptation the deflection of large-scale structures, and the alignment-free construction of structures from multiple starting locations. These benefits spurred the development of free-form [22] modular robots with arbitrary attachment locations, though such robots generally only operate in 2D, often have weak connections [23], [24], and often require specific alignment of the attachment mechanism to its neighbors' body [25], [26], [27], [28].

The second major design challenge for robotic selfassembling systems largely revolves around the locomotion of robotic agents. Popular approaches include relying on external forces [9], [18], using easily climbable passive members [17], [29], or relying on neighboring robots [14], [30]. Each approach simplifies robot design at the cost of reducing overall robot autonomy and introducing bottlenecks in the self-assembly process. In nature, self-assembling social insects move into position by climbing over their peers and autonomously deciding if and when to move. Implementing this challenging style of locomotion in robotics has yielded a variety of climbing techniques [8], [10], [25], [28], [31], [32]. Again, the style of attachment mechanism influences robot design: fixed-attachment-point robots must carefully consider the kinematics and motion of each step to ensure that attachment points are aligned [30], [33], whereas exact and precisely-controlled motion is less important when not requiring specific alignment between robots.

This letter presents FireAntV3 (see Fig. 1), a robot that innovates on the design of FireAnt3D [31] and explores how to incorporate sensors that might be useful in executing

2377-3766 © 2023 IEEE. Personal use is permitted, but republication/redistribution requires IEEE permission. See https://www.ieee.org/publications/rights/index.html for more information.



Fig. 1. FireAntV3 improves upon previous robots both through updated mechanical design as well as through expanded sensory capability. Each robot sphere is 65 mm in diameter.

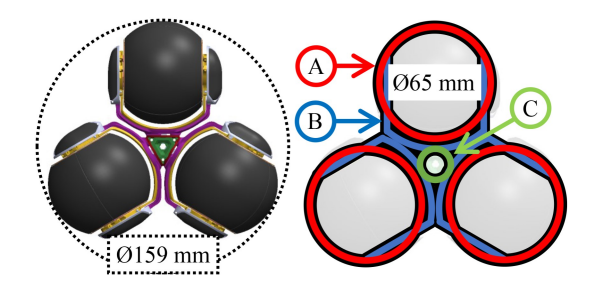


Fig. 2. FireantV3 consists of three general parts. Three spheres (A) mounted on forks (B) joined together at a central unit (C).

self-assembly algorithms. We organize the paper as follows: First, we present a high-level overview of the robot to contextualize subsequent sections. Next, we present an improved version of the Continuous Dock as well as its manufacturing method. We then describe the mechanical, electrical, and sensor design of the robot and describe and evaluate a neighbor-detection system. Finally, we demonstrate the above contributions on an autonomous robotic system and discuss areas for improvement through potential future work.

II. HIGH-LEVEL ROBOT OVERVIEW

As seen in Fig. 2, FireAntV3 consists of three spheres mounted on forks and joined by a centerbody. These spheres contain the majority of the system electronics and sensors and are coated in a continuous docking surface that allows peer robots to form strong attachments to each other regardless of the location or orientation of contact. Placing the spheres closely together helps ensure that any approach by a like robot will result in dock-to-dock contact, though this greatly constrains the size of the centerbody.

Using the continuous docks enables a simple form of locomotion first implemented in [31] (see Fig. 3) in which the robot first detaches its rear sphere, flips about its forward sphere (which is attached to another dock), then attaches on a newly forward sphere. This process requires no alignment between robots, enabling simple control with few sensors.

The new robot improves upon the design of its predecessor (FireAnt3D [31]) in several important ways. First, sphere diameter is reduced to 65 mm from 85 mm, giving an overall cylindrical envelope of 159 mm diameter × 65 mm height.

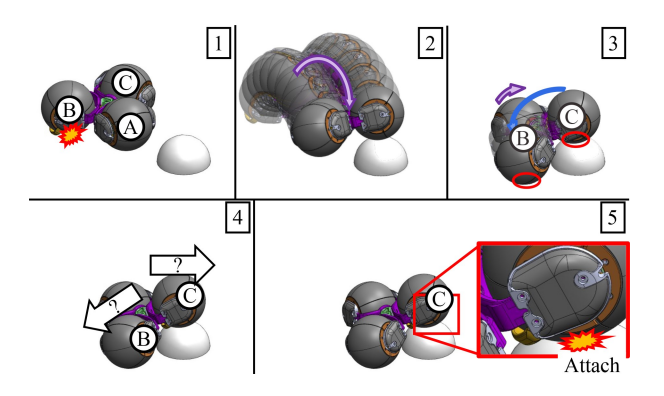


Fig. 3. Here, FireAntV3 has just flipped about sphere (B) and will move in the direction of sphere (A). Both (A) and (B) are attached to the environment. Locomotion proceeds in five phases: (a) FireantV3 detaches (B). (b) The robot flips about (A) until (c) it comes to rest on all three spheres. (d) FireAntV3 then decides the next direction of motion. (e) The robot attaches on the sphere associated with the desired direction.

These spheres are also supported on the sides (rather than the center), ensuring that docking material is present at the locations of most likely attachment. Finally, FireAntV3 uses a "hoop" to drive its flipping motion (rather than driving rotation of the dock directly, as with FireAnt3D), simplifying the design by reducing the number of motors from six to three. Note that despite this significant change, the locomotive process remains the same between FireAnt3D and FireantV3.

III. CONTINUOUS DOCKS

This section describes the Continuous Dock system [8], [31], [34], its principles of operation, and manufacture. These docks attach by passing current through conductive plastic to weld together, forming strong bonds between robots and enabling contacting robots to attach regardless of the exact position or orientation of contact. Robots using these docks can only attach to Continuous Docking surfaces, such as a self-assembled structure of robots using Continuous Docks or dock material implanted into the environment. These docks also take a long time to attach (approximately one minute), but the strength of the attachments is beyond the capabilities of other attach-anywhere mechanisms. In [31], we found that a three-dock to one-dock arrangement could withstand an average tensile force of 767 N (172 lb), a per-dock strength of 256 N (57 lb) (a conservative estimate of per-dock strength); we present no new testing data in this section.

A. Design and Principles of Operation

As illustrated in Fig. 4, the continuous dock mechanism has two main components: the docking surface itself and a ground-return hoop, a metal bar that the robot can move about the dock. The docking surface is a composite material consisting of a copper mesh sandwiched between two layers of electrically conductive, carbon-infused PLA plastic. This docking surface is mounted on a structural holder.

Fig. 5 illustrates the principle of operation of the 3D Continuous Dock. When two Continuous Docks come into contact the robot presses the docks together before executing a sequence of actions to weld the docks together. First, the copper mesh is energized to a nominal voltage of 33.3 V (the voltage of a



Fig. 4. (Left) The continuous docking surface (A), and the Aluminum ground-return hoop (B). (Right) The continuous docking surface is a composite material consisting of an outer 1.4 mm layer of conductive plastic (i), a copper mesh (ii), and a 0.2 mm second layer of conductive plastic. The composite is glued on a structural holder (iv).

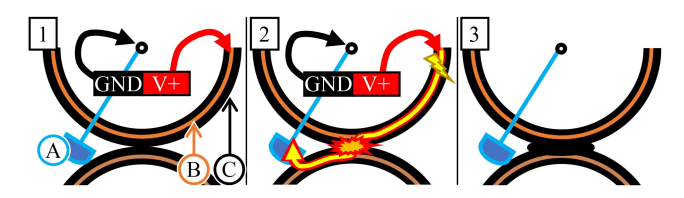


Fig. 5. Attachment of two Continuous Docks uses the ground-return hoop (A) and the docking surface consisting of copper mesh (B) and conductive plastic (C). Attachment is achieved using a simple procedure: (a) Sweep down hoop, (b) melt, (c) cool.

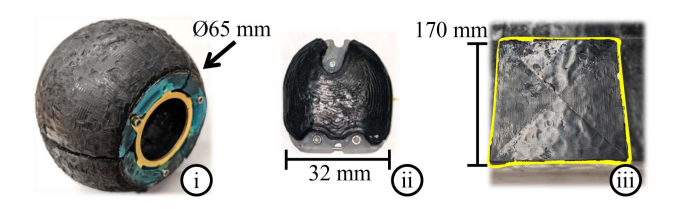


Fig. 6. Assembled set of spherical dock shells (a), a side shield (b), and an arena panel (c).

9S Li-Po battery) relative to the ground-return hoop. The hoop sweeps down until contact occurs between the ground-return hoop and the contacting dock. Current flows primarily along the copper mesh of the Continuous Dock until, to complete the circuit, it must pass through the higher resistance of the conductive plastic before eventually returning to ground via the hoop. This current heats and melts the plastic both on the active dock as well as on the contacting dock, but only at the point of contact: there is no perceptible heating of any other part of the robot. After passing 15 Amp-seconds (4.17 mAh) of time-integrated current the dock is de-energized and allowed to cool; the energy used in during attachment is less than 1% of robot battery capacity. The connection then cools for 40 s, yielding a strong and rigid bond. Detaching the docks uses a similar procedure, but melting serves to weaken the connection such that the docks can be separated without significant force.

Fig. 6 illustrates the three types of Continuous Dock used in this paper. Most attachments occur on the spherical shells, but we also affix "side shields" to robot spheres to ensure full coverage of the sphere. We also developed a Continuous Dock variant taking the form of $170 \, \mathrm{mm} \times 170 \, \mathrm{mm}$ squares which can serve as environmental anchors on which self-assembled structures could be built; we demonstrate the use of this dock type with the arena constructed for the experiments later in this paper. The variety of shapes and scales of these dock realizations demonstrates the geometrical flexibility of the 3D Continuous Dock.



Fig. 7. Major stages of Continuous Dock manufacture: (a) Printing blanks, (b) press-forming of the blank, (c) trimming and final assembly.

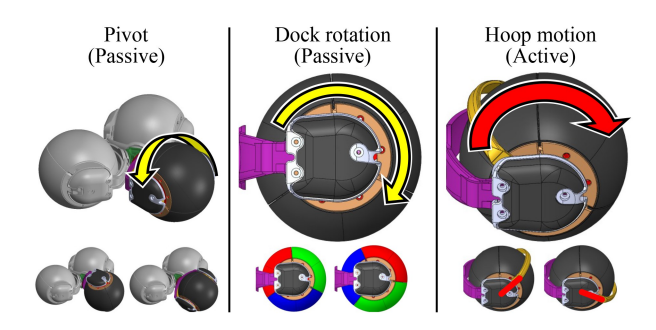


Fig. 8. Three degrees of freedom per sphere: (Left) Passive pivot, (Center) passive dock rotation spin, (Right) active driving of the hoop.

B. Manufacture of the Continuous Docks

The makeup and manufacture of the docking surfaces is the same regardless of the form that the Continuous Dock takes. Fig. 7 illustrates the main manufacturing steps. First, a single layer of conductive PLA is printed onto a build plate using an FDM 3D printer. The copper mesh is then placed on top of this single layer and taped to the build plate. A second print is then performed directly onto the copper mesh, allowing the extruded plastic to flow between the openings of the copper mesh and to attach to the first layer of plastic, minimizing the risk of delamination. Blanks are heated to 190 °C until pliable, then pressed in a silicone-lined mold. The dock then cools into its final shape before being trimmed to final dimensions and glued into a mounting structure.

IV. MECHANICAL DESIGN

FireAntV3 has three physical degrees of freedom per sphere (nine total) of which two are passive and one is active. Fig. 8 details these degrees of freedom. The first passive degree of freedom enables each sphere to pivot along the centerbody. The second passive degree of freedom enables the continuous dock to spin freely about the sphere. Finally, the active degree of freedom enables each sphere to drive the hoop continuously about the sphere. A photogate is used to detect when the hoop is returned to its "tucked" position under the fork. See Section IV-C for details on how FireAntV3 uses these degrees of freedom to locomote.

A. Centerbody Design

The centerbody holds the spheres close together and consists of three forks joined at the central (see Fig. 2). The central unit limits pivoting of these arms to $\pm 70^{\circ}$ and attaches to the forks using two screws apiece. Each fork has two force sensors (see Section VI-A) as well as light sensors (see Section VI-B). Six wires per sphere pass along these forks and through the central unit to electrically connect the entire robot. Rubber bands strung

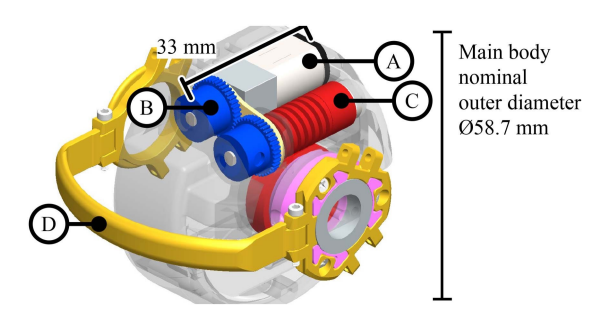


Fig. 9. Drivetrain of FireAntV3: A 380:1 gearmotor (A) drives spur gears (B) that turn a worm gear (C) and worm wheel combination with a ratio of 40:1. The worm wheel is attached to the hoop (D).

between these forks provide a passive return mechanism to return the forks to a neutral position when pivoted.

B. Sphere Design

The three robot spheres contain the majority of robot functionality. The 65 mm diameter of these spheres is determined by the thickness of the continuous docking material coating the spheres as well as the 450 mAh 3S Li-Po batteries that power the robot. These spheres also contain the drivetrain that moves the sphere's hoop (the active degree of freedom described in Fig. 8), as well as containing most of the robot's electronics. Spheres are interchangeable and mount to any of the three centerbody forks using three bolts.

The drivetrain of FireAntV3 (shown in Fig. 9) uses an N20 gearmotor to drive the hoop via a worm drive. This drivetrain makes use of off-the-shelf components wherever possible and has an overall gear ratio of 15200:1, approximately half that of FireAnt3D. This lower gear ratio was made possible by minimizing drivetrain friction using bearings and by increasing motor voltage from 5 V to 6 V. Further, the smaller overall size of the robot reduces the torque needed for the robot to apply a given press force, reducing the torque requirement.

C. Locomotion Detail

One of the primary innovations of FireAntV3 is the use of its Aluminum 3D-printed hoop to flip the robot rather than directly driving dock rotation, reducing the number of motors from six on the FireAnt3D robot to three on the FireAntV3 robot. To understand how the robot uses its hoop to flip, it is important to remember two properties of the robot: first, that the docking surface itself is free to spin relative to the rest of the robot; and second, that all other parts of the robot are essentially one piece. This means that when the motor moves the hoop, it moves that hoop relative to the rest of the robot but not necessarily relative to the dock. Thus, when there is an attached dock that the robot intends to flip about, moving the hoop downwards onto the surface and then continuing to move the hoop will push the hoop against the environment and thus begin to lift the robot. Fig. 10 illustrates this process. Further, by using the hoop to drive robot motion rather than directly driving the dock, stresses at the attachment location are approximately twelve times lower (see appendix for details), aiding robot locomotion reliability.

Despite this fundamental difference, FireAntV3's locomotive gait, discussed briefly in the robot overview section and illustrated in Fig. 3, is like that of FireAnt3D, where we demonstrated

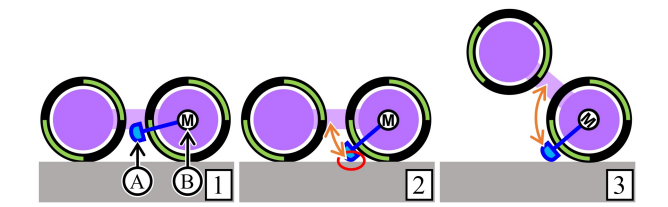


Fig. 10. FireAntV3 uses its hoop to flip: (a) The robot hoop (A) is driven by the motor (B), which is fixed to the main body of the robot (purple). (b) The robot moves the hoop downwards into contact with the environment. (c) The robot continues moving the hoop, allowing the robot to rotate within the passively-spinning continuous dock, lifting the robot from the surface.

that the gait enabled the robot to walk on arbitrary structures of like robots. Locomotion was demonstrated to be agnostic to the orientation of the surface the robot walks upon and does not require alignment or sensing, even to walk on complex arrangements of robots.

There are three general locomotive phases which, when repeated, enable the robot to move about arbitrary structures. In the discussion of these phases below, "aft sphere" refers to the sphere about which the robot has just flipped, i.e., the direction of the previous step. This sphere is still attached to the environment. "Flipping sphere" refers to the direction of the current step; this sphere is also attached to the environment. The phases of locomotion are as follows:

Detach: The aft sphere drives its hoop to press down the rest of the robot, compressing the connection on the flipping sphere to mitigate the tensile stresses experienced at that location. The aft sphere energizes its dock to melt its connection. At the same time, the forward dock pre-loads a lifting force using its hoop. When the connection of the aft dock has sufficiently weakened the aft sphere will detach.

Flip: The flipping sphere drives its hoop to flip the robot forward using the technique illustrated in Fig. 10. At the same time, the aft sphere stows its hoop in the gap between the docking surface and the fork. As the robot flips, one of the two non-flipping spheres will inevitably contact the environment before the other; when this happens, the robot continues flipping forward as the passive pivoting degree of freedom rotates; this pivoting enables all spheres to contact the environment. Flipping continues until the rotation speed (measured by the on-board gyroscope of the flipping sphere) falls below a threshold. At this point, the flipping sphere tares its force sensor and continues to flip forward until the robot is pressing down upon the surface with 9.8 N. During the flipping it is not uncommon for the passive rotation of the robot in the dock to outpace the rotation of the hoop, resulting in uncontrolled motion; this did not appear to negatively affect robot performance, however.

Attach: FireAntV3 steers by selecting the next sphere to flip about, then attaching on that sphere using the attachment process outlined in Section III-A.

Testing showed that refinements in robot design reduced step time by more than 75% compared to FireAnt3D. Table I summarizes the duration of the phases of locomotion. Note that while improved, attachment is still a long process due to the thermal nature of the docks.

 $\label{table I} TABLE\ I$ Comparison: Duration of the Phases of Robot Locomotion

Locomotion time properties (m:ss)			
	FireAntV3	FireAnt3D	Change
Time to detach	0:05	0:10	-0:05
Time to flip 180°	0:20	3:00	-2:40
Time to attach	1:05	3:20	-2:15
Overall step time	1:30	6:30	-5:00

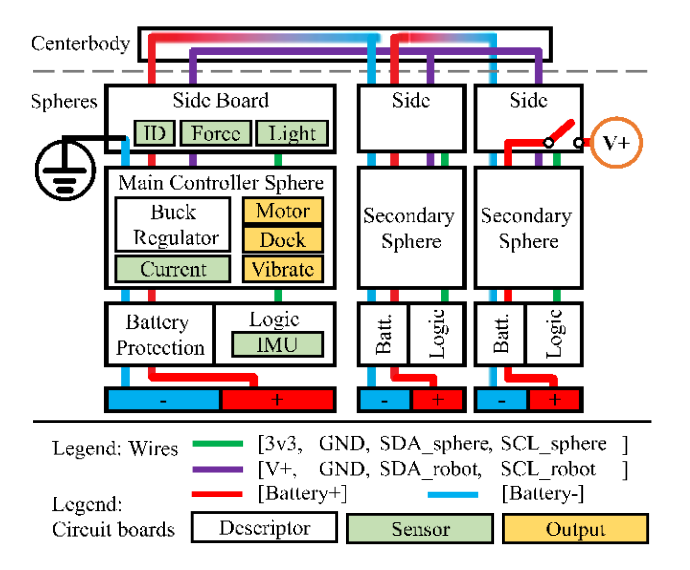


Fig. 11. Each sphere has a network of three circuit boards and a battery. Interconnect boards at the centerbody electrically connect the spheres. Functionality is only shown on the main controller sphere.

V. ELECTRICAL AND LOGICAL DESIGN

Fig. 11 summarizes the system electronics, which consists of three custom-designed PCBs per sphere (main, battery, and side boards), with each sphere operating semi-autonomously. Centerbody interconnect boards electrically join the spheres, connecting each sphere's 3S Li-Po battery in series, providing a total of 33.3 V with a system capacity of 450 mAh. At idle, the robot has a power draw of 45 mA, corresponding to approximately 10 hours of idle time.

Each sphere contains three circuit boards: one main board and two secondary boards. One of these secondary boards, located near the battery, contains battery protection circuitry as well as an IMU as well as a microcontroller for processing data from the IMU. The other secondary board resides on the side of the sphere and is responsible for force and light measurements. This side board is also the only circuit board with differentiation between spheres, and uses solder jumpers to define a unique ID for each sphere in the robot.

Spheres operate semi-autonomously, receiving high-level commands from a controller operating the sphere designated as the "main" sphere. This "main" sphere also uses a radio to enable interaction with and reporting to human operators. This hierarchical organization makes it straightforward to design robot behaviors by sequencing high-level sphere commands (e.g., "Attach" and "Flip").

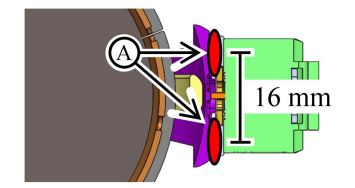
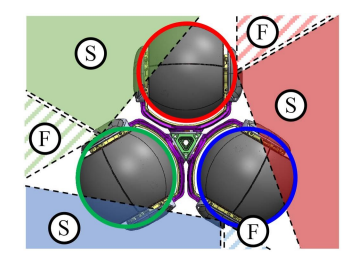




Fig. 12. (Left) Cross-section of the robot highlighting the position of the two force sensing resistors (A) on the centerbody forks. (Right) Highlights one of these force sensing resistors (B) as seen on a real robot.



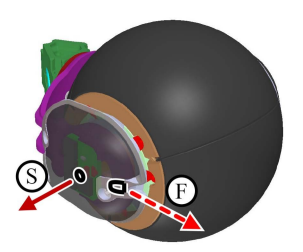


Fig. 13. Light sensors mounted on one side of each sphere look through holes in the continuous dock, with one sensor facing to the side of the sphere (S) and the other facing forward (F). Shaded regions correspond to the approximate field of view of each sensor (regions for (F) are hatch-shaded and (S) is solid) and colors correspond to the associated sphere.

VI. ROBOT SENSING

This section describes the major sensors used on FireAntV3. Robot sensing capabilities are based on what we expect to be necessary to implement the ReactiveBuild algorithm [7].

A. Force Sensing

Force sensing serves two main purposes: first, to allow the robot to detect the force with which it is pressing down during the attachment process; second, to sense structural forces during self-assembly (e.g., as required in the ReactiveBuild algorithm). The robot senses loads using a pair of force sensing resistors (FSR) with rubber domes over the sensing areas placed between the fork and central unit of the centerbody, as shown in Fig. 12. Because of how these two pieces are mated, the rubber domes are, in a neutral loading condition, compressed, meaning that each force sensing resistor can sense both an increase or decrease in load at their location (corresponding to different moment directions). Although FSRs are not as accurate or precise as solutions such as load cells or strain gages, they provide a compact and inexpensive solution with acceptable accuracy and precision, especially after post-assembly calibration.

B. Light Sensors to Sense Light Source-Based Goal Locations

Six photodiodes (two per sphere) enable FireAntV3 to determine the direction to a light source. Fig. 13 shows the placement of these light sensors on the robot. Since the robot can only ever step in one of three directions it is only necessary to determine which of the three spheres is closest to the light, rather than the precise direction of the light itself. The overlapping fields of view for the light sensors provide system redundancy and the 9-DoF IMUs in each sphere could also enable the robot to orient itself if the light source is occluded e.g., by another robot.

C. Vibration-Based Neighbor Sensing

FireAnt3D can detect surface contact using its force sensors, but these sensors cannot distinguish between the ground and other robots. This section presents a method for FireAntV3 robots to identify contact with other robots.

Robot-to-robot contact sensing is an ability often found in modular and reconfigurable robotic systems and is often used in the context of local robot-to-robot communication and coordination. In lattice-based modular robots, this contact sensing is often accomplished directly through a communication bus, since such robots are always guaranteed to attach at the same few locations. For free-form self-assemblages, however, this is not a viable option since attachment cannot be guaranteed to occur at discrete locations. Existing approaches to sensing contacts at arbitrary locations include use of magnetic sensor arrays [35], out-of-plane busses [23], and vibration sensing [25]. For FireAntV3 we pursued vibration-based sensing due to the minimal hardware requirements.

The methodology and results in this section are narrowly focused on exploring vibration-based neighbor detection in the context of the experimental setup and demonstrations discussed in the next section. Generalizing this work to account for different environmental vibration properties, arbitrary numbers of vibrating robots, and integration into a general-purpose communication system are outside the scope of the work presented in this paper. Instead, we concentrate on demonstrating that FireAntV3 is able to determine when it is contacting a vibration source versus when it is instead on the environment, as well as understanding how different contact conditions affect vibration measurements. Further, the quantitative results in this section correspond only to the sensing sphere shown in Fig. 14; vibration measurements for other spheres appeared to depend on exact robot positioning and were thus not repeatable, but were uniformly less than the vibrations measured by the sensing sphere.

FireAntV3 senses vibrations by looking at the change in measured accelerations between measurement updates, which occurred with a frequency of approximately 9.3 Hz (this update frequency was the maximum supported by the hardware configuration and was not a deliberate choice). In the absence of vibration, this value should be at or close to zero, with the IMU simply measuring the direction of gravity, whereas in a highvibration environment these values should increase due to the changing accelerations experienced by the robot. The specifics of vibration sensing differ between [25] and our implementation, since we measure vibration as the magnitude of change between consecutive measured 3D acceleration vectors, rather than only considering changes in the individual components of the acceleration vectors; our approach helps to eliminate differences in sensor effectiveness due to the orientation of the vibration. We also apply an exponential filter ($\alpha = 0.1$) to the magnitude of the vector difference to smooth this vibration measurement. To validate this methodology we performed an experiment (see Fig. 14) in which a FireAntV3 robot reported the vibrations it measured from a spare, continually-vibrating FireAntV3 sphere in several arrangements.

There are two main takeaways from these results. First and most importantly, there is a large difference in measured vibration between scenarios in which the measuring sphere of the FireAntV3 robot does not experience direct vibration (a,b) and scenarios in which the robot is either in contact with

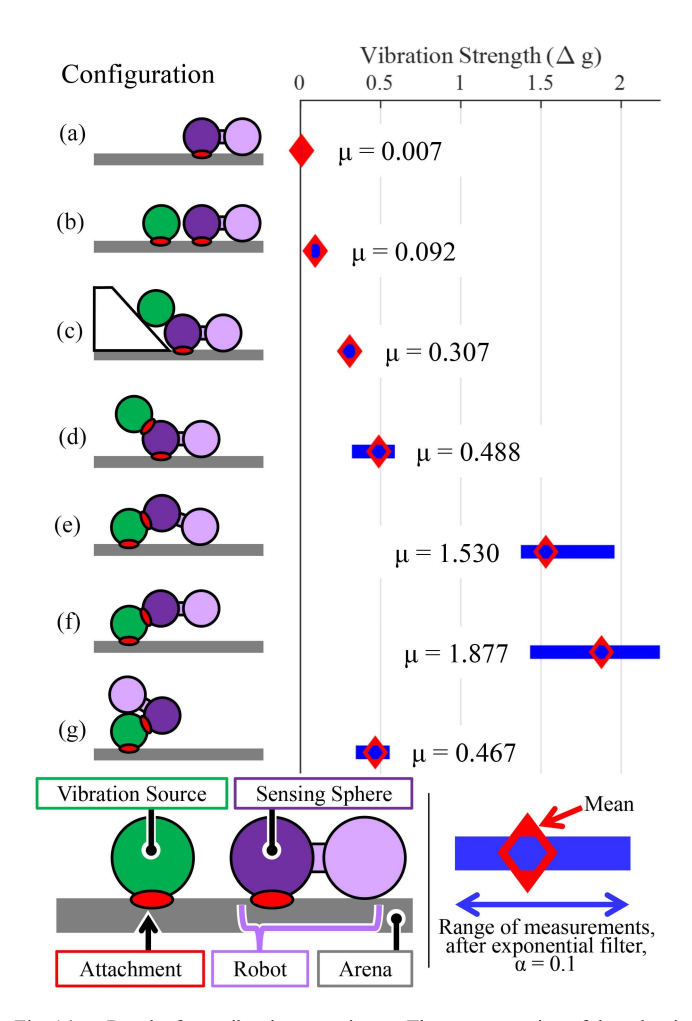


Fig. 14. Results from vibration experiment. The representation of the robot is simplified for the purposes of clarity; the dark purple (sensing) sphere is a single sphere, whereas the light purple circle represents the robot's other two spheres. Several configurations were tested: (a) No vibration present. (b) Vibrating sphere spaced approximately 1 mm away from FireAntV3. (c) Vibrating sphere placed on a 45 degree incline and allowed to roll into contact with FireAntV3. (d) Vibrating sphere attached to FireAntV3 in approximate position shown. (e)–(g) Represent various phases of a step.

the vibration source (c) or attached to the vibration source (d-g); this indicates that the FireAntV3 hardware is capable of vibration-based contact sensing, at least within the context of the tests performed in this paper. Second, we see that the overall strength of the observed vibration appears to be bimodal (compare (c,d,g) with (e,f)), possibly related to the number of contacts the overall robot makes with the vibrating sphere. This potentially has implications for vibration-based communication in large clusters of self-assembled robots, though future work will be required to understand these implications.

VII. TESTING AND DEMONSTRATIONS

This section demonstrates the sensory and locomotive capabilities of FireAntV3 on a flat arena consisting of nine 170 mm by 170 mm square continuous dock panels. The experiments in this section are intended to show these capabilities on a small scale with one robot (as with [31]), with the understanding that adjustments might be necessary in larger swarms. The tests also demonstrate the continuous dock panels, which will enable



Fig. 15. FireAntV3 executes phototaxis on the arena. Numbers correspond to individual steps.

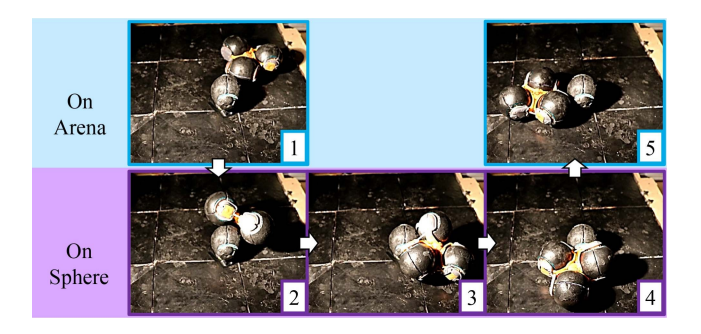


Fig. 16. FireAntV3 executes step-on-step-off on the arena. Images in the blue region show steps in which the robot did not detect the vibrating sphere and images in the purple region show steps in which the robots detected the vibrating sphere. The robot stopped when it detected that it has stepped off the vibrating sphere. Numbers correspond to individual steps.

robots to move about a simple, easily mountable surface prior to beginning a self-assembled structure.

A. Phototaxis

Phototaxis is a behavior in which a robot moves towards a light source. This enables users to set a goal location for robots to move towards, an ability that can be useful in self-assembly algorithms such as ReactiveBuild [7]. This demonstration shows the autonomous locomotion of FireAntV3, its light-sensing capabilities, as well as that the square dock panels can be used as an environment that robots can walk upon.

In a dark room, a FireAntV3 robot was placed on one end of the arena and a halogen light source was placed on the opposite end of the arena. No effort was made to orient the robot in any particular direction. The robot successfully executed phototaxis until the robot has crossed the arena in a series of five steps, as shown in Fig. 15.

B. Step-On, Step-Off

Step-on, step-off behavior involves two robotic elements: one fully functional FireAntV3 robot and one robot sphere that outputs a vibration signal. The robot executes phototaxis until it first climbs atop this robotic sphere (sensed via the presence of a vibration signal), then climbs off the sphere and back onto the arena (sensed via the absence of a vibration signal) then stops. Based on the vibration tests described earlier, the robot used a threshold value of 0.3 to determine whether it was contacting the vibrating sphere. The ability for the robot to detect whether it was on or off the vibrating sphere was evident both through changes to its behavior as well as changes in wireless debug reports. Fig. 16 shows this experiment. This demonstration again shows the locomotive capabilities of FireAntV3, as well

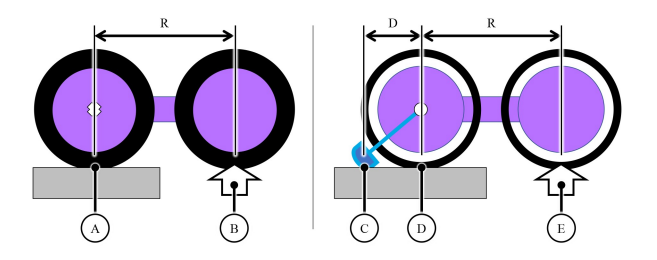


Fig. 17. (Left) A dock-driven robot (FireAnt3D) has docks (black circles) fixed to the robot (purple). The environment-dock interface (A) resists the reaction force and bending moment induced by force $F_{applied}$. (Right) A hoop-driven robot (FireAntV3) has docks that rotate freely about the robot. $F_{applied}$ (E) is counteracted by the hoop-environment interface (C) as well as the dock-environment interface (D), resulting in higher tensile forces at (D), but no bending moment.

as demonstrating the real-world application of vibration-based neighbor detection.

While successful, this test revealed several potential challenges of vibration-based communication. One such issue was the impact of the vibration on measuring forces and using the IMU to measure flip speed. To ignore transient measurements while the logic waits for measurements to meet some threshold, we require that measurements exceed thresholds for several measurement cycles before acting on the measurements. A larger issue was the increased difficulty in sensing when the hoop had actually contacted the vibrating sphere, likely because the vibration causes spheres to bounce off each other slightly; because the hoop contact sensing relies on detecting a small 0.005 A current, inconsistent contact can defeat this detection. A future robot could address this issue either through increasing the press force prior to attachment, or though using different means of detecting hoop contact.

VIII. CONCLUSION

FireAntV3 is a significant step forward towards the realization of real-world free-form and environment-adaptive self-assembly and has demonstrated how free-form robots can sense aspects of the environment as well as the presence of contacting neighbors. The capabilities demonstrated in this letter bring the FireAnt robot hardware much closer to being capable of executing the ReactiveBuild algorithm [7] for use with FireAnt-style robots. One of the most significant capabilities yet to be demonstrated using these robots is robot-robot communication; for future work, we propose that one way robots could communicate with each other would be to use a hybrid local-global communication system in which robots would identify neighbors by first signalling globally that they are about to identify themselves, then emitting a vibration pulse to allow neighboring robots to determine if they are in contact. Other future work towards demonstrating self-assembly will also require resolving the challenges associated with forming connections to vibrating neighbors, exploring ways in which these robots could operate in arbitrary, out-of-lab environments, and further improving attachment time.

APPENDIX

Comparison of locomotion stresses for two approaches to driving motion (see Fig. 17). Equation (1): connection stress

on a robot where the dock is driven to exert a torque (as in FireAnt3D). Equation (2): connection stress on a robot where the hoop is driven to exert a torque (as in FireAntV3). Derivation of these equations is left to the reader. **Assumptions:** Ignore friction, circular attachment with radius r, system is infinitely stiff. **Representative measurements:** $R = 0.07 \, \text{m}$, $r = 0.005 \, \text{m}$, and $D = 0.018 \, \text{m}$. **Result:** Hoop-drive design has stresses approximately 12 times lower than those of dock-drive. **Discussion:** Although the presented model is greatly simplified this is unlikely to impact the overall takeaway of the calculation: the use of the hoop as the primary method of moving the robot vastly improves attachment loading conditions. Calculations match qualitative observations.

$$\sigma^{tensile, overall, dockdrive} = \frac{F_{applied}}{\pi r^2} \frac{4R}{r} + 1 \qquad (1)$$

$$F_{applied}R + D$$

$$\sigma^{tensile, overall, hoopdriven} = \frac{\pi r^2}{r} \frac{D}{r} \qquad (2)$$

REFERENCES

- [1] C. R. Reid, M. J. Lutz, S. Powell, A. B. Kao, I. D. Couzin, and S. Garnier, "Army ants dynamically adjust living bridges in response to a cost–benefit trade-off," *Proc. Nat. Acad. Sci.*, vol. 112, no. 49, pp. 15113–15118, 2015.
- [2] T. Bochynek, F. Schiffers, A. Aichert, O. Cossairt, S. Garnier, and M. Rubenstein, "Anatomy of a superorganism-structure and growth dynamics of army ant bivouacs," 2021, arXiv:2110.09017.
- [3] O. Peleg, J. M. Peters, M. K. Salcedo, and L. Mahadevan, "Collective mechanical adaptation of honeybee swarms," *Nature Phys.*, vol. 14, no. 12, pp. 1193–1198, 2018.
- [4] C. Anderson, G. Theraulaz, and J.-L. Deneubourg, "Self-assemblages in insect societies," *Insectes Sociaux*, vol. 49, pp. 99–110, 2002.
- [5] K. H. Petersen, N. Napp, R. Stuart-Smith, D. Rus, and M. Kovac, "A review of collective robotic construction," *Sci. Robot.*, vol. 4, no. 28, 2019, Art. no. eaau8479.
- [6] M. Yim et al., "Modular self-reconfigurable robot systems [grand challenges of robotics]," *IEEE Robot. Automat. Mag.*, vol. 14, no. 1, pp. 43–52, Mar. 2007.
- [7] P. Swissler and M. Rubenstein, "ReactiveBuild: Environment-adaptive self-assembly of amorphous structures," in *Proc. Int. Symp. Distrib. Auton. Robot. Syst.* 2021, pp. 363–375.
- [8] P. Swissler and M. Rubenstein, "FireAnt: A modular robot with full-body continuous docks," in *Proc. IEEE Int. Conf. Robot. Automat.*, 2018, pp. 6812–6817.
- [9] J. Neubert, A. P. Cantwell, S. Constantin, M. Kalontarov, D. Erickson, and H. Lipson, "A robotic module for stochastic fluidic assembly of 3D self-reconfiguring structures," in *Proc. IEEE Int. Conf. Robot. Automat.*, 2010, pp. 2479–2484.
- [10] J. W. Romanishin, K. Gilpin, S. Claici, and D. Rus, "3D M-blocks: Self-reconfiguring robots capable of locomotion via pivoting in three dimensions," in *Proc. IEEE Int. Conf. Robot. Automat.*, 2015, pp. 1925–1932.
- [11] N. J. Mlot, C. A. Tovey, and D. L. Hu, "Fire ants self-assemble into waterproof rafts to survive floods," *Proc. Nat. Acad. Sci.*, vol. 108, no. 19, pp. 7669–7673, 2011.
- [12] P. C. Foster, N. J. Mlot, A. Lin, and D. L. Hu, "Fire ants actively control spacing and orientation within self-assemblages," *J. Exp. Biol.*, vol. 217, no. 12, pp. 2089–2100, 2014.
- [13] F. Scholz, "Tolerance stack analysis methods," Research and Tech., Boeing Information Support Services, Boeing, Seattle, WA, USA, 1995.

- [14] H. Kurokawa, K. Tomita, A. Kamimura, S. Kokaji, T. Hasuo, and S. Murata, "Distributed self-reconfiguration of M-TRAN III modular robotic system," *Int. J. Robot. Res.*, vol. 27, no. 3/4, pp. 373–386, 2008.
- [15] A. Spröwitz, R. Moeckel, M. Vespignani, S. Bonardi, and A. J. Ijspeert, "Roombots: A hardware perspective on 3D self-reconfiguration and locomotion with a homogeneous modular robot," *Robot. Auton. Syst.*, vol. 62, no. 7, pp. 1016–1033, 2014.
- [16] U. A. Fiaz and J. S. Shamma, "Usbot: A modular robotic testbed for programmable self-assembly," *IFAC-PapersOnLine*, vol. 52, no. 15, pp. 121–126, 2019.
- [17] J. Werfel, K. Petersen, and R. Nagpal, "Designing collective behavior in a termite-inspired robot construction team," *Science*, vol. 343, no. 6172, pp. 754–758, 2014.
- [18] K. Gilpin, A. Knaian, and D. Rus, "Robot pebbles: One centimeter modules for programmable matter through self-disassembly," in *Proc. IEEE Int. Conf. Robot. Automat.*, 2010, pp. 2485–2492.
- [19] J. Baca, S. Hossain, P. Dasgupta, C. A. Nelson, and A. Dutta, "ModRED: Hardware design and reconfiguration planning for a high dexterity modular self-reconfigurable robot for extra-terrestrial exploration," *Robot. Auton.* Syst., vol. 62, no. 7, pp. 1002–1015, 2014.
- [20] M. Rubenstein, K. Payne, P. Will, and W.-M. Shen, "Docking among independent and autonomous CONRO self-reconfigurable robots," in *Proc. IEEE Int. Conf. Robot. Automat.*, 2004, pp. 2877–2882.
- [21] N. J. Wilson, S. Ceron, L. Horowitz, and K. Petersen, "Scalable and robust fabrication, operation, and control of compliant modular robots," *Front. Robot. AI*, vol. 7, 2020, Art. no. 44.
- [22] K. Gilpin and D. Rus, "Modular robot systems," *IEEE Robot. Automat. Mag.*, vol. 17, no. 3, pp. 38–55, Sep. 2010.
- [23] M. Shimizu and A. Ishiguro, "An amoeboid modular robot that exhibits real-time adaptive reconfiguration," in *Proc. IEEE/RSJ Int. Conf. Intell. Robots Syst.*, 2009, pp. 1496–1501.
- [24] S. Li et al., "Particle robotics based on statistical mechanics of loosely coupled components," *Nature*, vol. 567, pp. 361–365, 2019.
- [25] M. Malley, B. Haghighat, L. Houe, and R. Nagpal, "Eciton robotica: Design and algorithms for an adaptive self-assembling soft robot collective," in *Proc. IEEE Int. Conf. Robot. Automat.*, 2020, pp. 4565–4571.
- [26] F. Mondada et al., "SWARM-BOT: A new distributed robotic concept," Auton. Robots, vol. 17, pp. 193–221, 2004.
- [27] D. Zhao and T. L. Lam, "SnailBot: A continuously dockable modular self-reconfigurable robot using rocker-bogie suspension," in *Proc. Int. Conf. Robot. Automat.*, 2022, pp. 4261–4267.
- [28] G. Liang, H. Luo, M. Li, H. Qian, and T. L. Lam, "FreeBOT: A freeform modular self-reconfigurable robot with arbitrary connection point-design and implementation," in *Proc. IEEE/RSJ Int. Conf. Intell. Robots Syst.*,2020, pp. 6506–6513.
- [29] N. Melenbrink, P. Michalatos, P. Kassabian, and J. Werfel, "Using local force measurements to guide construction by distributed climbing robots," in *Proc. IEEE/RSJ Int. Conf. Intell. Robots Syst.*, 2017, pp. 4333–4340.
- [30] F. Wang, Z. Qian, Z. Yan, C. Yuan, and W. Zhang, "A novel resilient robot: Kinematic analysis and experimentation," *IEEE Access*, vol. 8, pp. 2885–2892, 2020.
- [31] P. Swissler and M. Rubenstein, "FireAnt3D: A 3D self-climbing robot towards non-latticed robotic self-assembly," in *Proc. IEEE/RSJ Int. Conf. Intell. Robots Syst.*, 2020, pp. 3340–3347.
- [32] L. Cucu, M. Rubenstein, and R. Nagpal, "Towards self-assembled structures with mobile climbing robots," in *Proc. IEEE Int. Conf. Robot. Automat.*, 2015, pp. 1955–1961.
- Automat., 2015, pp. 1955–1961.
 [33] T. Zhang, W. Zhang, and M. M. Gupta, "An underactuated self-reconfigurable robot and the reconfiguration evolution," Mechanism Mach. Theory, vol. 124, 248–258, 2018.
- [34] P. Swissler and M. Rubenstein, "Method and system for joining robotic components," U.S. Patent 11,305,421, Apr. 2022.
- [35] Y. Tu, G. Liang, and T. L. Lam, "Graph convolutional network based configuration detection for freeform modular robot using magnetic sensor array," in *Proc. IEEE Int. Conf. Robot. Automat.*, 2021, pp. 4252–4258.